Engineering formula for pressure loss in an oscillating-triangular-jet nozzle

P. V. Lanspeary[1] **and S. K. Lee**[1]

[1]School of Mechanical Engineering
University of Adelaide, Adelaide, South Australia, 5005 AUSTRALIA

Abstract

A nozzle consisting of a circular inlet orifice and a short chamber with an exit lip can produce a naturally oscillating jet flow if the expansion ratio from inlet to chamber (D/d_1) is larger than five. As an industrial natural-gas burner, the device offers advantages over simple nozzles of equivalent capacity. However, its usefulness as a pulverised solid-fuel burner is constrained because it requires a high supply pressure. This is due to the high energy-loss coefficient of the inlet expansion ratio, D/d_1. If an equilateral-triangular inlet replaces the circular inlet, oscillating flow occurs at equivalent expansion ratios as low as $D/d_1 \approx 2$, and the supply pressure is much lower.

An engineering model of the loss coefficient is obtained from measurements of supply pressure over a wide range of nozzle geometries. To begin, we split the overall loss coefficient K into three components, one for each of the inlet orifice, chamber and exit lip. A formula representing each component of K is then determined from dimensional analysis, inspection of the data, and least-squares curve fitting. Combining these component formulae gives K as a function of four geometric parameters and seven numerical coefficients. When the numerical coefficients are optimised simultaneously, the r.m.s. difference between the model and the data is 2.2%.

Introduction

Nathan et al. [4] have shown that a nozzle consisting of a circular inlet orifice and a chamber with an exit lip can produce a naturally oscillating jet flow. This device is known as the "fluidic-precessing-jet" (FPJ) nozzle because flow from the inlet orifice (Figure 1) is deflected asymmetrically toward the wall of the chamber, and the direction of deflection changes with time so that the reattached jet travels or "precesses" around the wall. In the initial studies, Nathan et al. [4] found that the range of chamber geometries which produce an oscillating jet is quite narrow; the diameter expansion ratio from orifice to chamber should be larger than five ($D/d_1 \gtrsim 5$), and the length ratio of the chamber should be in the range $2.6 \lesssim L/D \lesssim 2.8$.

At an early stage, the FPJ nozzle was developed as an industrial natural-gas burner because the flame is shorter, more luminous and more resistant to "blow-off" than equivalent simple turbulent-jet or "axial-jet" nozzles [6]. The higher luminosity, which is due to the large-scale oscillation of the FPJ flow, can lead to a decrease of as much as 40% in nitrogen-oxide (NO_x) emissions [7]. Initial experience with FPJ burners in cement
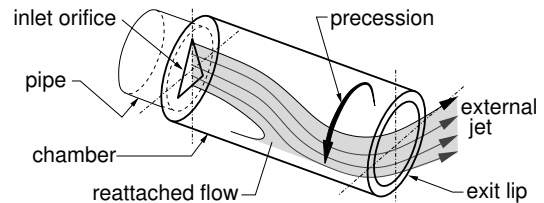

Figure 1: Fluidic-precessing-jet nozzle.

Figure 2: Oscillating-triangular-jet nozzle.

kilns showed that, along with advantages such as reduced NO_x and improved product quality, there are some features which may act as limitations. The most intractable of these is the effect of the geometric criterion $D/d_1 \geq 5$ on the trade-off between fuel-supply pressure and the size of the burner: an FPJ burner requires a much higher fuel pressure than an axial-jet burner of the same outer diameter and flow rate.

Mi et al. [3] found that an FPJ-like flow oscillation is obtained with a number of different inlet orifice-shapes. In particular, with an equilateral-triangular orifice (Figure 2) the jet oscillates at expansion ratios as low as $D/d_1 \approx 2$. This allows the triangular-jet nozzle to have a larger inlet orifice than the FPJ nozzle, and so the flow-energy loss coefficient is much lower. In some applications this would be a significant benefit because it either reduces the cost of pumping the flow through the nozzle, or it allows a corresponding reduction in the size of the nozzle and its supporting structure.

Lee et al. [2] have performed a parametric study of the "oscillating-triangular-jet" (OTJ) nozzle. Their results verify that oscillation occurs at much smaller expansion ratios than in the FPJ nozzle and that the necessary supply pressure is much lower. They also show that, unlike an FPJ, oscillation is continuous rather than intermittent. The parametric study shows that the jet spreading angle is smaller than for the FPJ, and varies more gradually over a wide range of L/D ratios and inlet-expansion ratios (Figure 3). A designer therefore has the flexibility not only to accommodate a much lower supply pressure, but also to choose the jet spreading angle.

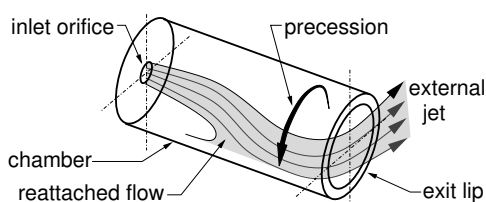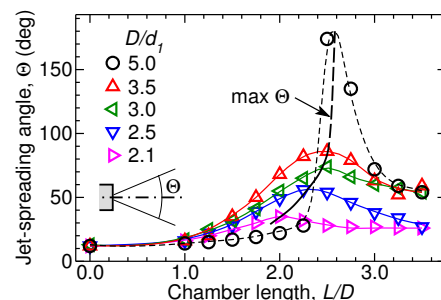This paper provides a formula which gives an engineering ap-

Figure 3: Spreading angle of the OTJ, observed with a streamer at the exit plane of the nozzle — from Lee et al. [2].
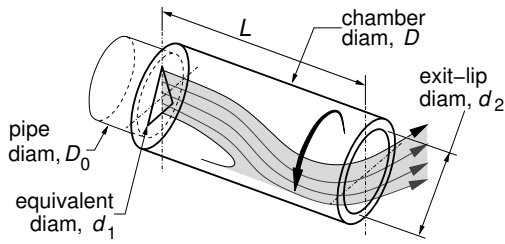
Figure 4: Geometric parameters.

proximation to the flow-energy loss or pressure loss of the oscillating-triangular-jet (OTJ) nozzle. The flow is incompressible; inlet-orifice Reynolds numbers (Re_1) are between 3,800 and 60,400.

Experimental Method

Figure 4 defines the geometric parameters of the OTJ nozzle. The size of the triangular orifice is given as the "equivalent diameter" d_1 of a circular orifice of the same area. The inlet orifice is cut from flat plate.

Figure 5 is a diagram of the apparatus. The air supply for the nozzle is taken from a 200 c.f.m. (340 m^3/hr), 700 kPa industrial air compressor and is regulated to 210 kPa in the laboratory. The OTJ nozzle is connected to a smooth-wall tube of internal diameter $D_0 = 0.753D$ and length $50D_0$. Flow passes through a honeycomb and wire-mesh screen before entering the tube. The tube provides the OTJ nozzle with inlet-flow conditions which are a close approximation to a fully developed pipe flow [2].

The dimensionless parameter which describes the flow-energy loss is the "loss coefficient"

$$K = \frac{P_0 - P_\infty}{\frac{1}{2}\rho U_0^2} + 1, \tag{1}$$

where P_∞ is pressure in the ambient fluid. Bulk-mean flow speed, U_0 is measured with a 19 mm (3/4-inch) float/tube flow meter. The static pressure difference $P_0 - P_\infty$ is measured $10D_0$ upstream of the triangular orifice in order to avoid error due to streamline curvature near the orifice and error due to azimuthal pressure variations. The energy-loss coefficient (due to wall friction) of 10 diameters of smooth pipe (≈ 0.3) is negligible in comparison with the loss coefficient of the OTJ nozzle. The results of the measurements are shown in Figure 6.

Initial Analysis

The most important feature of Figure 6(a) is that the loss coefficients of the OTJ nozzle are much lower than the loss coefficient of the FPJ nozzle. This difference occurs because the triangular nozzle has a smaller contraction ratio (D_0/d_1) from inlet pipe to orifice. The loss coefficient depends much less strongly on other geometric parameters of the nozzle. Figure 6(b) shows that increasing chamber length from zero to $L/D = 2.25$ produces a
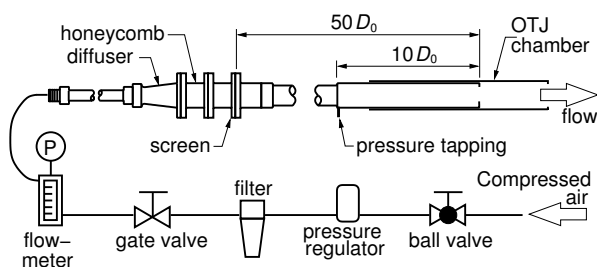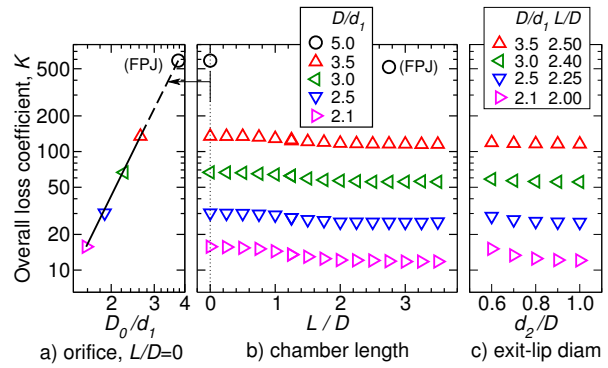

Figure 5: Apparatus.

Figure 6: Measurements of OTJ ($\triangle$, $\triangleleft$, $\triangledown$, $\triangleright$) and FPJ ($\bigcirc$) loss coefficient (K) as functions of (a) orifice contraction ratio (D_0/d_1) at $L/D = 0$, (b) chamber length (L/D) with $d_2/D = 0.9$, and (c) exit lip diameter (d_2/D). $Re_1 = 50,000$

pressure recovery (i.e. decrease in K) of between 13% and 23%. Pressure recovery may be due to flow reattachment inside or at the exit lip of the chamber. The lip itself (Figure 6(c)) has an even smaller effect. Figure 6 suggests that the overall loss coefficient should be written as the sum of three components:

$$K = K_o + K_c + K_l, \tag{2}$$

where K_o is the loss due to flow contraction at the orifice, K_c is a "negative loss" due to a relatively small diffuser-like pressure recovery over the length of the chamber, and K_l is due to the exit lip. From dimensional analysis the OTJ loss coefficient and each of its components are functions of 4 geometric parameters and Reynolds number:

$$K = K_o + K_c + K_l = \mathbf{f}\left(\frac{D_0}{d_1}, \frac{D}{d_1}, \frac{L}{D}, \frac{d_2}{D}, Re_1\right). \tag{3}$$

Reynolds number is defined in terms of flow conditions at the inlet orifice, $Re_1 = U_1 d_1/\nu$. By fitting mathematical functions of these parameters to each of the experimentally measured K_o, K_c and K_l, we obtain an engineering formula or model of the overall loss coefficient.

Effect of Reynolds Number

Loss coefficient has been measured over the Reynolds-number range $3,800 < Re_1 < 60,400$, with a chamber length of $L = 2.75D$ and an exit-lip diameter of $d_2 = 0.9D$. As functions of Reynolds number, variations in loss coefficient are so small that they would not be visible on the log-scale of Figure 6. The results are therefore shown in Figure 7 as discharge coefficient. Discharge coefficient is defined as the actual flow rate divided
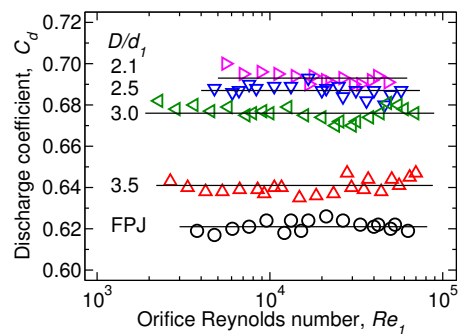

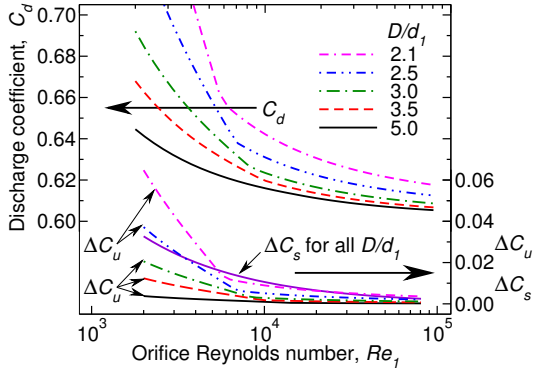Figure 7: Discharge coefficient (C_d) as a function of orifice Reynolds number. $3,800 < Re_1 < 60,400$.

Figure 8: Reader-Harris [8] formula for orifice-plate discharge coefficient (C_d) as a function of **orifice** Reynolds number (Re_1) and diameter ratio (D/d_1). Pressure tappings are distances D upstream and $D/2$ downstream of the orifice plate. Reynolds-number dependent terms ΔC_u and ΔC_s are shown on a shifted vertical scale. A rapid change of slope can occur at laminar-turbulent transition (at pipe-flow Reynolds number, $Re_0 = 4{,}000$).

by the flow rate through a lossless contraction with the same pressure difference and diameter ratio. It is calculated from the loss coefficient and the contraction ratio using

$$C_d = \sqrt{\frac{1}{K-1}\left[\left(\frac{D_0}{d_1}\right)^4 - 1\right]}. \qquad (4)$$

With the exception of the smallest expansion ratio ($D/d_1 = 2.1$), a 95%-confidence-level test indicates that the measurements have not detected a Reynolds-number dependence in the discharge coefficient. Horizontal lines of best fit are included in Figure 7 as a visual guide.

Figure 8 shows the Reader-Harris [8] formula for the discharge coefficient of a circular orifice plate in a fully developed pipe flow. The formula was obtained by curve fitting to a database of 16,376 experimental measurements and it is a further development of the Reader-Harris/Gallagher formula which is recommended by ISO-5167.2 [1] for measurement of flow rate in pipes. The Reader-Harris [8] formula has several Reynolds-number dependent terms. The two largest of these are shown as ΔC_u and ΔC_s in Figure 8. The ΔC_u term accounts for the effect of Reynolds number on the velocity profile in the upstream pipe flow. In the OTJ flow, this effect would appear in K_o. The second term, ΔC_s represents Reynolds-number effect in the separated and reattaching flow downstream of the orifice. For the OTJ, this effect would appear in K_c. Since both ΔC_u and ΔC_s have negative slope, we conclude from Figure 7 that neither K_o nor K_c depend on Reynolds number.

Effect of Inlet-orifice Contraction

If the chamber is removed (i.e. $L/D = 0$), the jet flow from the inlet orifice is unconfined and, since the effect of Reynolds number is negligible, the energy-loss coefficient is a function of only one parameter, the contraction ratio D_0/d_1:

$$K_o = K|_{L/D=0} = \mathbf{f}_1\left(\frac{D_0}{d_1}\right). \qquad (5)$$

Figure 6(a) shows that a least-squared curve fit of the form

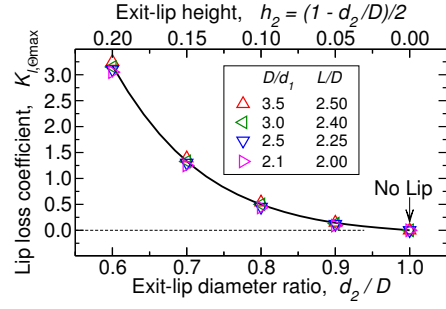$$K_o = \kappa \left(\frac{D_0}{d_1}\right)^\zeta \qquad (6)$$

Figure 9: Energy-loss coefficient of the exit-lip at maximum spreading angle of the emerging jet flow, $Re_1 = 50{,}000$. Equation 7 is shown as solid line.

is appropriate for the "$L/D = 0$" experimental data. With $\kappa = 2.04$ and $\zeta = 4.28$, the r.m.s. difference between Equation 6 and the data is about 2.6%.

Effect of Exit-Lip Diameter

Figure 9 shows the component of loss coefficient (K_l), due to the exit lip. For each of the available expansion ratios (D/d_1), K_l was measured at the chamber length giving the largest spreading angle (Θ_{max}) of the emerging jet [2]. Given a required jet spreading angle, these chamber geometries minimise the energy loss of the nozzle. The range of exit-lip diameters is limited to $0.6 \le d_2/D \le 1.0$ because, for lip diameter smaller than $0.6D$, the external flow does not oscillate. Figure 9 indicates that the loss coefficient of the exit lip (K_l) is independent of both the contraction ratio (D_0/d_1) and the expansion ratio (D/d_1) at the inlet orifice. The data in Figure 9 falls on the curve

$$K_{l,\Theta_{max}} = h_2 \cdot \left[353 h_2^2 + 1.40\right], \qquad (7)$$

where $h_2 = [1 - (d_2/D)]/2$ is the dimensionless height of the lip, with an r.m.s. difference of $\Delta K_l \approx 0.08$.

Effect of Chamber Length and Expansion Ratio

Figure 6 shows that the chamber behaves like a weak diffuser. The chamber produces a small pressure recovery between the inlet orifice of the nozzle and the exit plane. In Equation 3 this pressure recovery or reduction in energy-loss coefficient is written as a function of the inlet contraction ratio (D_0/d_1), expansion ratio (D/d_1) and chamber length (L/D). However, if the loss coefficient of the chamber (K_c') is defined with a reference flow speed U_{vc}, which is the flow speed at the vena contracta just downstream of the inlet orifice, we would expect it to be independent of the inlet contraction ratio:

$$K_c' = \frac{\Delta P_c}{\frac{1}{2}\rho U_{vc}^2} = \mathbf{f}_2\left(\frac{D}{d_1}, \frac{L}{D}\right), \qquad (8)$$

where ΔP_c is the pressure loss attributable to the chamber and $\mathbf{f}_2$ is a "chamber-loss function". Converting from a vena-contracta reference speed to an inlet-pipe-flow reference speed gives

$$K_c = \left(\frac{U_{vc}}{U_0}\right)^2 \cdot K_c' = \left(\frac{U_{vc}}{U_0}\right)^2 \cdot \mathbf{f}_2\left(\frac{D}{d_1}, \frac{L}{D}\right). \qquad (9)$$

Boundary friction and turbulence-energy dissipation of the flow contraction through the inlet orifice are negligible and so, in Equation 9, the ratio $(U_{vc}/U_0)^2$ is the loss coefficient of the inlet-orifice contraction:

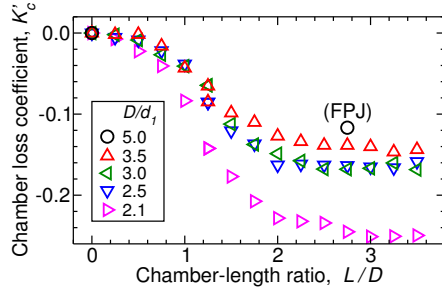$$K_c = K_o \cdot K_c' = K_o \cdot \mathbf{f}_2\left(\frac{D}{d_1}, \frac{L}{D}\right). \qquad (10)$$

Figure 10: Chamber-loss coefficient K'_c based on flow speed at the vena contracta. $Re_1 = 50,000$, $d_2/D = 0.9$.

The numerical values of K'_c in Figure 10 are obtained from the experimental data (K) by using

$$K'_c = \frac{K - K_o - K_l}{K_o}, \qquad (11)$$

where K_o is given by Equation 6. For these measurements the exit diameter is $d_2 = 0.9D$, and so the lip-loss coefficient K_l is negligible. Figure 10 suggests that the chamber-loss function $\mathbf{f}_2$ should consist of two factors, an "amplitude-of-decay" factor which depends on the expansion ratio and a "decay-rate" factor which depends on chamber length:

$$\mathbf{f}_2\left(\frac{D}{d_1}, \frac{L}{D}\right) = \underbrace{\left[-\beta\left(\frac{D}{d_1}\right)^{\eta}\right]}_{\text{amplitude}} \cdot \underbrace{\left[1 - \exp\left(-\left[\frac{1}{\lambda}\frac{L}{D}\right]^{\xi}\right)\right]}_{\text{decay-rate factor}}. \quad (12)$$

Figure 11 explains the effect of each curve-fitting coefficient (β, η, λ and ξ) on the shape of the function, $\mathbf{f}_2$.

Optimising the Model

The formula for the overall loss coefficient of the nozzle is obtained by substituting Equations 6, 10, and 12 into Equation 3:

$$K = \kappa\left(\frac{D_0}{d_1}\right)^{\zeta}\left\{1 - \beta\left(\frac{D}{d_1}\right)^{\eta}\left[1 - \exp\left(-\left[\frac{1}{\lambda}\frac{L}{D}\right]^{\xi}\right)\right]\right\} + K_l. \quad (13)$$

An initial estimate of the coefficients κ, ζ, β, η, λ and ξ can be obtained by minimising the mean-squared-error of fits to subsets of the data. First, contraction coefficients κ and ζ are found from the "$L/D = 0$" data (Figure 6(a)). The coefficients β and η are then calculated from the amplitude of the decay in K'_c (Figure 10). Finally, the remaining coefficients λ and ξ are obtained from the decay rate of the K'_c data.

The coefficients of the model are optimised by the downhill-simplex method of Nelder and Mead [5]. By minimising the mean-square of the percentage difference between the model (Equation 13) and the measurements shown in Figure 6(b), we obtain

$$K = K_l + 2.21\left(\frac{D_0}{d_1}\right)^{4.213} \times \qquad (14)$$

$$\left\{1 - 0.421\left(\frac{D}{d_1}\right)^{-0.85}\left[1 - \exp\left(-\left[\frac{1}{1.42}\frac{L}{D}\right]^{2.8}\right)\right]\right\}$$

The number of digits in each optimised numerical coefficient in Equation 14 is chosen so that changing a least significant digit alters the value of K by less than 1%. Figure 12 compares Equation 14 with the experimental data. The r.m.s. difference between the model (Equation 14) and the data (Figure 6(b)) is 2.3%. The maximum difference is 4.4%.
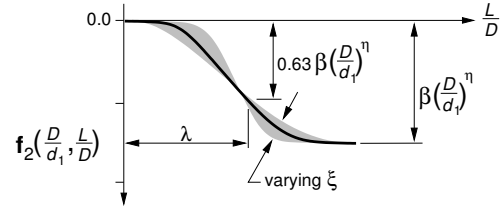

Figure 11: Sketch of the chamber-loss function, $\mathbf{f}_2$.

References

[1] ISO (International Standards Organization), *ISO 5167.2-2003, Measurement of fluid flow by means of pressure differential devices inserted in circular cross-section conduits running full – Part 2: Orifice plates*, 2003.

[2] Lee, S. K., Lanspeary, P. V., Nathan, G. J., Kelso, R. M. and Mi, J., Low kinetic-energy loss oscillating-triangular-jet nozzles, *Experimental Thermal and Fluid Science*, **27**, 2003, 553–561.

[3] Mi, J., Nathan, G. J., Luxton, R. E. and Luminis Pty. Ltd., Naturally oscillating jet devices, Australian Patent Office, Patent Application No. PP0421/97, 1998.

[4] Nathan, G. J., Hill, S. J. and Luxton, R. E., An axisymmetric 'fluidic' nozzle to generate jet precession, *Journal of Fluid Mechanics*, **370**, 1998, 347–380.

[5] Nelder, J. A. and Mead, R., A simplex method for function minimization, *Computer Journal*, **7**, 1965, 308–313.

[6] Newbold, G. J. R., Nathan, G., Nobes, D. S. and Turns, S. R., Measurement and prediction of NO_X emissions from unconfined propane flames from turbulent-jet, bluff-body, swirl, and precessing jet burners, in *Twenty-Eighth International Symposium on Combustion*, Edinburgh, Scotland, 2000, 481–487.

[7] Rapson, D., Stokes, B. and Hill, S. J., Kiln flame shape optimisation using a Gyro-Therm gas burner, *World Cement*, **26**, 1995, 2–5.

[8] Reader-Harris, M. J., Sattary, J. A. and Spearman, E. P., The orifice plate discharge coefficient equation — further work, *Flow Measurement and Instrumentation*, **6**, 1995, 101–114.
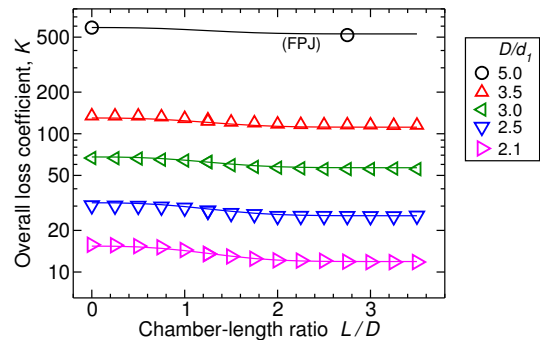
Figure 12: Comparison of loss-coefficient model (Equation 14) with the experimental data. Equation 14 is shown as solid lines. The experimental data are shown as symbols, $\bigcirc, \triangle, \triangleleft, \triangledown, \triangleright$.